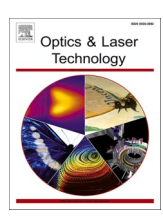
ELSEVIER

Contents lists available at ScienceDirect

Optics and Laser Technology

journal homepage: www.elsevier.com/locate/optlastec



Full length article



Design and fabrication of photonic crystal structures by single pulse laser interference lithography

Zhiheng Lin, Yun-Ran Wang, Yaoxun Wang, Mark Hopkinson

Department of Electronic and Electrical Engineering, The University of Sheffield, Sir Frederick Mappin Building, Sheffield S1 3JD, UK

ARTICLE INFO

Keywords:
Photonic Crystal
Laser interference lithography
Semiconductors
Antireflection
Photovoltaics

ABSTRACT

Photonic crystal (PhC) structures formed by periodic surface nanostructuring have emerged as pivotal elements for controlling light-matter interactions. One important application is reducing losses due to the high surface reflectivity of semiconductor optoelectronic devices, such as enhancing light absorption in photovoltaic cells or improving light extraction in light-emitting diodes (LEDs). Although various methods for fabricating such structures have been documented, the utilization of single pulse laser interference lithography (LIL) using commercial photoresist and its subsequent effective use as an etch mask has not been previously reported. Rapid exposure of photoresists with single nanosecond pulses offers benefits for high throughput patterning and reduces the requirement for a stable optical platform. We have successfully employed single pulse LIL to fabricate antireflective PhC structures on GaAs substrates using a commercial photoresist. Exposure is performed with single 7 ns 355 nm pulses of relatively low energy (<10 mJ). High-quality nanohole arrays of pitch of approximately 365 nm are fabricated and depths up to 400 nm have been etched using inductively coupled plasma (ICP) through the exposed photoresist mask. Reflectivity analyses confirmed that these structures reduce the average reflectance of the GaAs to below 5 % across the 450 nm to 700 nm visible wavelength range. The fabrication of PhC structures using this approach has potential for low-cost wafer-level patterning to provide improved light extraction in LEDs and enhanced light trapping in solar cells.

1. Introduction

Extensive applications of surface nanostructuring have been pursued to improve the energy conversion efficiency of semiconductor photonic devices including solar cells, light-emitting diodes (LEDs), and laser diodes (LDs) [1–4]. Amongst the materials employed in the fabrication of such semiconductor optoelectronic devices, Si and GaAs stand out as prominent examples. In contrast to Si, GaAs exhibits a direct bandgap, an elevated breakdown voltage, high thermal stability, and noteworthy radiation resistance characteristics which result in remarkable stability even within challenging operational environments [5-8]. However, GaAs, as well as other semiconductors exhibit a high surface reflectivity which reduces the external efficiency of these devices. In GaAs, the reflectivity exceeds 39 % in the visible spectrum, whilst for Si this is only slightly better at around 37 %. Surface reflectivity therefore has a significant impact on the external quantum efficiency of these devices and methods to control this are as important as the device structure and materials properties. In the context of GaAs solar cells, the power conversion efficiency is currently capped at approximately 17.57 % [9]. Whilst in the realm of GaAs LEDs, the external efficiency is constrained to a mere 3 % [10].

Due to the high intrinsic reflectivity, surface engineering techniques such as antireflective coatings (ARCs) [11–15] or surface nanostructuring [16–18] are a key requirement for high-performance devices. ARCs can provide a simple means to mitigate surface reflection losses and angular reflectivity dependence, which affects photovoltaic systems, the light extraction efficiency in LEDs, and can enhance the contrast and brightness in display technologies [19]. However, for an ARC to realize wideband antireflectance needs a careful selection of materials with specific refractive indices and precise calibration of layer thicknesses. This elevates the complexity of the ARC fabrication process which invariably leads to increased processing time and cost, both in the developmental phase and in the actual manufacturing of these multilayered coatings [14,20–23].

As an alternative, top-down surface nanostructuring encompassing periodic PhC structures has been shown to provide broadband and wide-angle incident light antireflectance, coupled with a substantial reduction in radiant heat transmission [24]. Commonly known as 'Moth Eye'

E-mail address: m.hopkinson@sheffield.ac.uk (M. Hopkinson).

^{*} Corresponding author.

structures, these can be engineered to achieve a substantial reduction in spectral reflectance over a wide spectral range, extending from the visible ($\sim\!400$ nm) to the mid-infrared region (up to $11~\mu m$), with reflectance values achievable as low as 2 % [25,26,32]. In addition, PhCs exhibit a more expansive versatility in the manipulation of light, finding profound applications beyond simple antireflection. PhCs achieve this by manipulating light propagation within their periodic nanostructures, thereby facilitating innovative approaches in the control and direction of light for various technological applications [4,27]. These applications encompass advanced fields such as LEDs [28,29], solar cells [3,4], telecommunications [30], sensors [31], and other optical devices.

A multitude of methods have been established for the successful synthesis of PhC structures. These include electron beam lithography (EBL) [32,45] and nanoimprint lithography (NIL) [34–36]. Whilst these methods are effective, they are often burdened by substantial cost implications and low throughput. In contrast, laser interference lithography (LIL) [33,38–42] is lauded for its simplicity and cost-efficiency, mitigating financial constraints typically associated with nanofabrication. Moreover, it is recognized for its temporal efficiency, enabling rapid fabrication processes. Additionally, its potential to pattern over large areas further enhances its applicability in industrial-scale production [37–39]. Extensive research reveals instances of fabricating PhC structures using LIL on a variety of materials, such as Si [40], polymer [41], and WO₃ [42].

There are some similarities between our work and previous studies, such as Dong et al [26] who have created columnar moth- eye structures through exposed photoresist using laser interference and then etch. We also note that Martín-Fabiani et al [41] have structured thin polymer films to depths ~200 nm. However, their methodology uses CW lasers with exposure times in the second range using commonly available mW-output UV lasers. We use a single pulse Q-switched laser providing fewnanosecond single pulses in the tens of millijoule range. To our knowledge this has not been performed before for complete device fabrication. We believe the fast pulse approach offers a potentially very high throughput in which a whole wafer could be exposed on a timescale only limited by the wafer step and repeat translation. The use of nanosecond pulses also significantly reduces stage vibration concerns and may present advantages in terms of photoresist thermal damage.

There is one report on the exposure of photoresist using nanosecond pulses by Ellman et al [38]. The paper demonstrated high quality 2D photoresist arrays. However, the focus of their paper is more to study the effect of laser conditions, and they have not explored the use of the resulting pattern as an etch mask. As a result, there is no study of the resulting optical properties. Also, the pitch of their 2D patterns is considerably larger (850 nm).

In this work, we use single pulse three-beam laser interference lithography (LIL) for the fabrication of PhC structures on GaAs substrates, followed by inductively coupled plasma (ICP) etching to create nanoholes of varying depths. We observe that these surface PhC nanoholes significantly improve light extraction and trapping capabilities within the corresponding wavelength ranges for which we have simulated the photonic band gap (PBG). In addition, our surface reflectivity measurement demonstrates a substantial decrease in average reflectance, with values falling below 4 % across the visible wavelength range of 400–700 nm. This investigation into the reflectivity modifications resulting from PhC formation seeks to unravel the mechanisms by which these nanostructures augment optical performance. Understanding these interactions is essential for the optimization of existing photonic technologies and could be instrumental in the advancement of future devices characterized by enhanced light management properties.

2. Design of PhC structures by LIL

In this research, the LIL system is a core element of the experimental scheme. This system operates using a flash-lamp pumped Nd: YAG laser

(Innolas Spitlight) which is characterized by the following operational parameters: a wavelength of 355 nm, a frequency of 5 Hz, a pulse duration of 7 ns, and a beam diameter of 5 mm. The laser is vertically polarised. This laser serves as the primary source for generating interference patterns.

Fig. 1 shows the three-beam LIL setup. The operational mechanism of the LIL system involves the division of the laser beam into three equal beams through the utilization of beam splitters. Compared to the commonly used four-beam setup, the three-beam asymmetric arrangement can avoid the effect of long range modulation due to the Moiré effect [39]. The three beams are subsequently recombined onto the surface of the sample. In this setup, the angle of incidence of three beams is set to be 43° and the azimuth angles are set at 0°, 90°, and 180°, respectively. Precise alignment of the laser beams is imperative for achieving the targeted nanostructure configuration. This is achieved through imaging the UV pulse via an InGaN wafer, which provides not only a downshift of the emission into the blue, but also has a luminescence decay which enhances the timescale for CMOS camera capture. The resultant pattern is designed to exhibit the required periodicity and uniformity, attributes that are crucial for the intended application. The pulse energy is adjusted using an integral attenuator based on a polarizer/wave plate configuration and was measured by a calibrated thermopile sensor (Ophir 7Z02622 3A-P) before splitting into 3 beams.

According to the foundational principles of LIL, which have been extensively discussed in our preceding publications [39,43], the pattern formation employing a three-beam LIL configuration was simulated using plane wave calculations in MATLAB. This simulation is integral to the planning of the PhC structure process. Fig. 2a and b show 2D and 3D simulations of the laser intensity distribution. The shape of the final PhC structure is determined by this pattern, which adheres to the principles outlined in Eq. (1). Eq. (2) elucidates a correlation between the pitch (P) of the interference pattern and the angle of incidence laser beam (θ) .

$$I = \left| \sum_{i=1}^{n} A_m \overrightarrow{P_m} \exp \left[i \left(\overrightarrow{k_m} * \overrightarrow{r} + \delta_m \right) \right] \right|^2$$
 (1)

$$P = \frac{\lambda}{\sqrt{2}\sin\theta} \tag{2}$$

In Eq. (1), the symbol I stands for the intensity of the light pattern resulting from the interference of multiple laser beams. m is the number of the beams, where A_m signifies the amplitude, $\overrightarrow{P_m}$ denotes the polarization vector, $\overrightarrow{k_m}$ represents the wave vector indicating the direction of propagation, \overrightarrow{r} is the position vector and δ_m signifies the initial phase.

The distinctive characteristic of PBGs has become a significant element in modern nanophotonic design. The pitch of PhC structures and the size of the nanoholes play an essential role in determining the PBG. GaAs-based light-emitting devices commonly operate in the visible to the near-infrared spectrum, typically around 850 nm to 1500 nm.

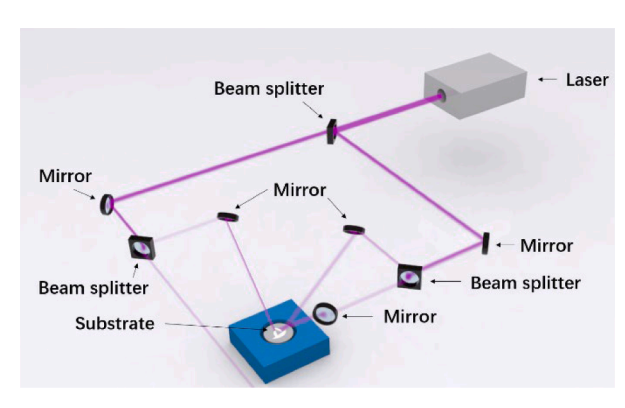


Fig. 1. Three-beam LIL setup.

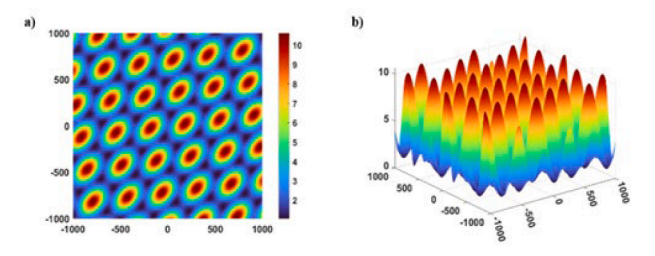


Fig. 2. a) 2D, b) 3D laser intensity distribution pattern.

Therefore, an incidence angle of 43° is selected to obtain a pitch size of around 365 nm.

3. Experimental details

The experimental procedure is shown in Fig. 3.

GaAs substrates were subjected to a three-step cleaning protocol (Acetone, Isopropanol, DI water rinse) and then spun dry. After prebaking, a 180 nm-thick film of mr-P 1200LIL photoresist (Microresist technology GmbH) was applied to the substrates by spin-coating.

This photoresist is specifically developed for laser lithography applications and provides high contrast for a thin film thickness. Previous experiments with more standard greyscale lithography photoresists at higher thicknesses (1.5–2.5 μ m) proved ineffective due to difficulties in exposing to the total depth of the photoresist. These leaves residues which then cannot be completely removed It is important to note that we can always expose the photoresist to a greater depth using a higher laser pulse power. However, the photoresist is subject to laser-induced damage at high energy regime (>15 mJ). This thin and high-contrast photoresist makes it possible to totally remove the exposed area in the developer solution whilst using relatively low energy pulses (~10 mJ).

Following this, the photoresist was patterned using single pulse three-beam LIL to define the desired pattern. The exposed sample is developed in a metal ion bearing, silicate/phosphate-based developer (ma-D 374/S- Microresist technology GmbH) for durations of 30 s-1 min. Pattern transfer to the wafer is subsequently achieved using ICP etching with a Cl/Ar chemistry (Oxford instrument Plasmapro). The etching rate was maintained at 200 nm per minute. By controlling the etching duration, PhC samples with various etch depths have been fabricated. The etch depth is contained within the 800 nm p-type contact layer in the epitaxial structure.

4. Results and discussion

4.1. Structural analysis

Fig. 4 shows SEM images of GaAs surfaces featuring PhC structures

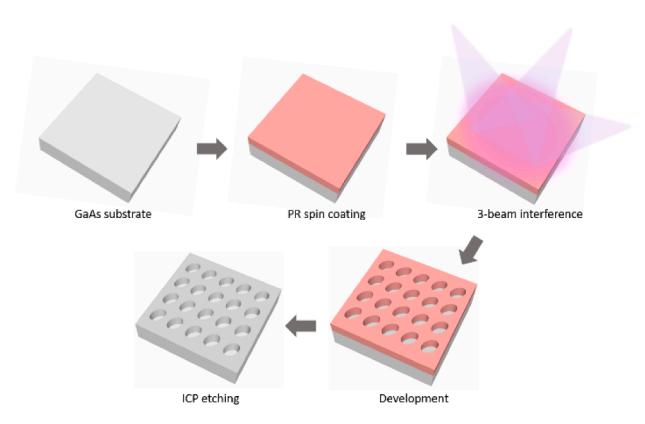


Fig. 3. The fabrication process of the PhC structures

after etching, captured at varied magnifications. The images demonstrate uniform periodically aligned nanoholes over a significant area.

The pitch between the nanoholes measures approximately 365 nm, a dimension that is consistent with the outcomes derived from MATLAB simulations of laser interference.

The diameter of each nanohole is influenced by the laser energy applied during the lithographic process. Adjusting the radius of the holes (r) in relation to the pitch (P), as well as considering the refractive index contrast between the holes and the surrounding membrane, provides a mechanism to manipulate the PBG's characteristics. Specifically, a smaller r/P ratio results in a narrower Photonic Band gap (PBG) which increases linearly with this ratio. Furthermore, elevating the air content in the structure by increasing the radius amplifies the central bandgap frequency. However, escalating the radius leads to heightened loss rates due to reduced guiding material and fabrication challenges due to intricate features between larger holes [44]. Consequently, a compromise arises between the bandgap size and practical limitations. The size of r depends on the laser intensity. A high laser intensity can lead to the connection of adjacent nanoholes in certain regions. This agglomeration disrupts the intended architecture of the PhC structure. Conversely, insufficient laser intensity can result in inadequate exposure of the resist's full depth, leading to residual material that hampers effective etching. To strike an optimal balance, a laser energy of 9 mJ was selected for this process, forming more satisfactory PhC structures.

Under three beam exposure, the nanoholes assume an elliptical shape, with the ellipse's major axis reaching a maximum diameter of $\sim\!\!315$ nm and a minor axis with a diameter of $\sim\!\!300$ nm. We have analysed the variation in the dimension of the etched holes by edge detection and the resulting distribution is shown in Fig. 4d. The standard deviation in the major axis is 11 nm. This may be an overestimate due to inaccuracies in the edge detection. It shows the ability to produce regular etched holes with a low ($\leq\!3\%$) dimensional variation.

4.2. Photonic band gap of the 2D PhC

The periodicity of the PhC (which defines the Brillouin zone) leads to Bragg scattering and wave interference, which in turn results in the formation of distinct PBGs. The formation of PBGs is intimately linked to the structure of the Brillouin zone shown in Fig. 5a. The wave vectors within the square Brillouin zone follow the path Γ XM Γ . Fig. 5b shows the outcomes of the simulation of the PBG using the Finite-Difference Time-Domain (FDTD) method (Ansys Lumerical).

This simulation provides an understanding of the relationship between the size and pitch of the nanoholes and the propagating optical wavelengths. The normalised frequency corresponds to the quantity (a/ λ), where a is the period or lattice constant of the PhC and λ the wavelength of the light. The dispersion diagram manifests a PBG in two distinct spectral regions: firstly, between the normalized frequencies of 0.28 to 0.31, and secondly, from 0.38 to 0.44. The 2D PhC structure under consideration operates efficiently as an out-coupler for transverse electric (TE) guided modes within these PBG regions.

Note the change to normalised units (pitch/wavelength) in Fig. 5b comes from $\omega a/2\pi c=a/\lambda.$ The pitch (a) of 365 nm corresponds to λ between 830–960 nm. The significance of these wavelength ranges lies in their alignment with the emission wavelengths of several semiconductor devices. Specifically, the range from 830 nm to 960 nm coincides with the emission wavelengths prevalent in GaAs/InGaAs based LEDs, and LDs. Moreover, the longer wavelength range of 1177 nm to 1303 nm corresponds to the O-band, which is known for its reduced dispersion and attenuation in optical fibres, making it an optimal choice for long-distance and high-fidelity data transmission.

4.3. AFM and reflectance results analysis

The reflectance of the fabricated PhC structures at different depths was characterized using a silicon CMOS array detector spectrometer

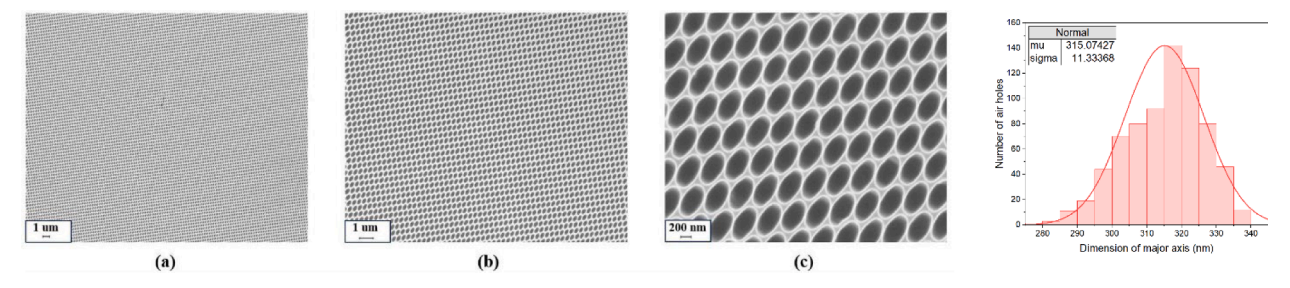
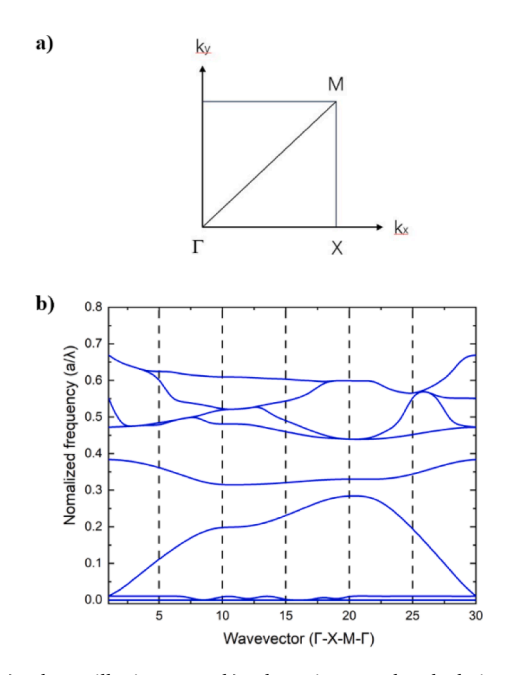


Fig. 4. a), b), c) SEM images of etched PhC structures at different magnifiantions. d) Distribution of the major axis dimension of the etched holes.



 $\label{eq:Fig. 5.a} \textbf{Fig. 5. a)} \ \ \text{The Brillouin zone, b)} \ \ \text{Photonic crystal calculation obtained from FDTD.}$

integrated into an optical microscope with visible illumination ranging from 450 nm to 700 nm. This setup, as we have previously reported [45], allows the measurement of the reflectance of each pattern with different depths. Precise positioning of the sample is ensured by a panning stage, which enables precise measurements of each pattern through the microscope. Through the microscope's aperture control, illumination can be focused on the pattern area. For light collection, a 50x microscope objective with a numerical aperture (NA) of 0.56 and a 33.3° half-cone angle was used.

We have contrasted the reflectivity properties of GaAs substrates, both with and without embedded PhC structures, across varying etch depths. Employing the ICP etching technique, a series of PhC structures were fabricated at specified depths of 80 nm, 200 nm, 300 nm, 350 nm, and 400 nm. The topographical features of these structures were delineated through AFM measurements, shown in Fig. 6. Note from AFM measurements, we estimate that the unpatterned surface has an RMS roughness of <5 nm. From simulations, this will not have a significant impact on the reflectance. Reflectance spectra obtained from these samples are illustrated in Fig. 7.

The bare GaAs substrate exhibited a high average reflectance, measuring as high as 39 % within the wavelength range from 450 nm to 700 nm. This high reflectance is attributable to the refractive index contrast between air ($\eta=1$) and GaAs ($\eta=3.8$), the high semiconductor values being quite typical across a range of materials. It is important to note that PhC structures do not intrinsically modify this high refractive index contrast; rather, they leverage it to intricately manipulate light

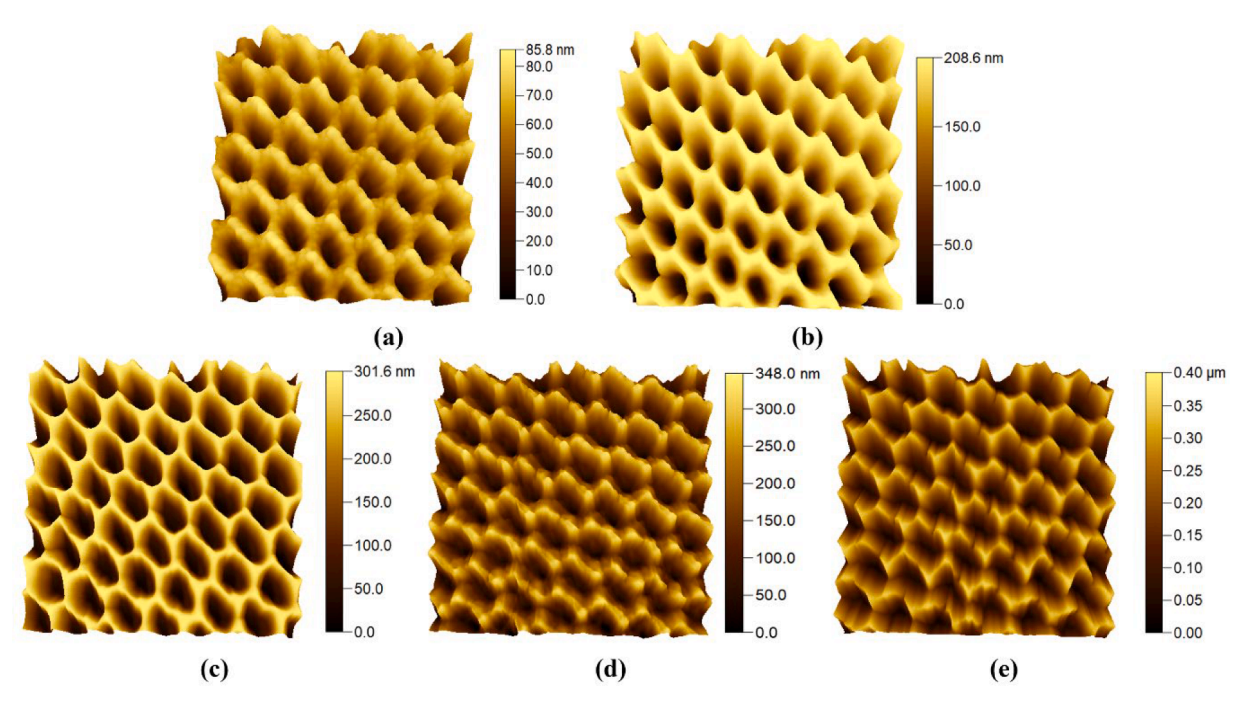


Fig. 6. a) 80 nm, b) 200 nm, c) 300 nm, d) 350 nm, e) 400 nm depths PhC structure on GaAs substrate.

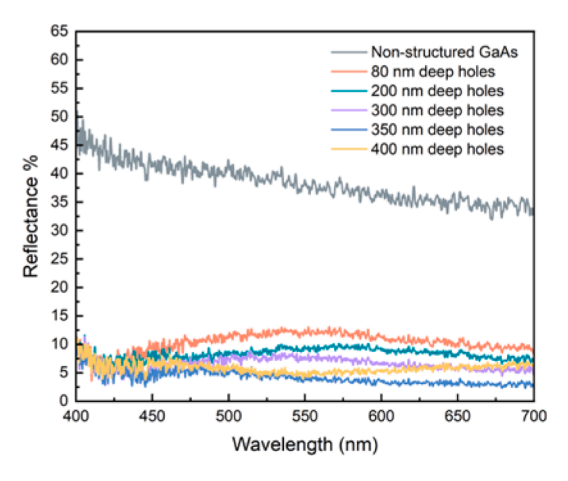


Fig. 7. Comparative analysis of reflectance between bare GaAs substrates and GaAs substrates embedded with PhC structures ranging in depths from 80 nm to 400 nm.

propagation, thereby achieving a reduction in surface reflectivity.

A key observation in our study was the role of the depth of the PhC structures in influencing reflectivity. The reflectance data in Fig. 7 shows a trend concerning the depth of nanoholes in the PhC structures and their corresponding impact on reflectivity. It is discernible from the data that an increment in the depth of the nanoholes is associated with a decrease in reflectivity from 80 nm to 350 nm depths. When the depth of the nanoholes attains 350 nm, the average reflectance diminishes to below 5 % across the spectral range, which spans from 400 nm to 700 nm. This represents a sevenfold reduction in reflectance when compared to GaAs lacking the PhC structure.

We observe that augmenting the depth of PhC structures enhances the capacity for light trapping. This enhancement occurs as incident light traverses an extended path within the material, thereby amplifying the probability of light absorption. Furthermore, an increase in the depth of the PhC structures contributes to the optimization of Bragg scattering phenomena. This phenomenon, arising from the periodic architecture of the crystal, induces diffraction of light, culminating in either constructive or destructive interference. This strategic interference effectively diminishes the proportion of light that is reflected from the surface. Additionally, these diffraction effects can be engineered to redirect light away from the surface, thereby reducing reflectivity.

However, at depths of 400 nm, the reflectivity did not follow the previous pattern of a continuous decline and instead there was a slight increase in reflectivity. The depth may reach a point where it negatively impacts light trapping or introduces unwanted diffraction effects, altering the reflectivity in undesired ways.

5. Conclusions

In this work, we have designed and fabricated PhC structures on GaAs substrates, employing the technique of single pulse LIL. The surface morphology of the fabricated PhC structures was validated to adhere to our initial design through SEM and AFM analyses. We conducted FDTD simulations to map the PBG properties of these PhC structures. The results reveal that the PhC structures exhibit the potential to be integrated into GaAs-based optoelectronic devices. This integration is projected to enhance their performance, providing gain within specific wavelength ranges. Additionally, our experimental measurements have determined that the average reflectance of the GaAs substrates equipped with PhC structures can be significantly reduced to below 5 % across a broad wavelength spectrum of 450 nm to 700 nm. Therefore, the PhC structure delineated in this research can enhance the light extraction efficiency in light-emitting devices and increase light trapping efficacy for photovoltaic applications.

Single pulse LIL is adaptable to a variety of semiconductor materials, enabling the creation of highly efficient optoelectronic devices optimized for broadband applications. To achieve a wafer level process,we would need to expand the beam using appropriate optics and employ step and repeat with a suitable translational stage. The short pulse timescale (~7ns) can enable several patterns per second with the only limitation being the speed of the translational stage. The use of this technology, characterized by its cost-effective and high-throughput approach, has significant potential to contribute to technological progress in the field of photonics and optoelectronics.

CRediT authorship contribution statement

Zhiheng Lin: Writing – original draft, Visualization, Investigation. Yun-Ran Wang: Writing – review & editing, Project administration, Investigation. Yaoxun Wang: Investigation. Mark Hopkinson: Writing – review & editing, Supervision.

Declaration of competing interest

The authors declare that they have no known competing financial interests or personal relationships that could have appeared to influence the work reported in this paper.

Data availability

Data will be made available on request.

Acknowledgments

The authors gratefully acknowledge financial support from EPSRC (Grant: EP/X016838/1) and the Grantham Foundation Opportunities Fund

For the purpose of open access, the authors have applied a Creative Commons attribution (CC BY) licence to the accepted manuscript.

References

- [1] C. Ducros, A. Brodu, G. Lorin, F. Emieux, A. Pereira, Optical performances of antireflective moth-eye structures. Comparison with standard vacuum antireflection coatings for application to outdoor lighting LEDs, Surf. Coat. Technol. 379 (2019), https://doi.org/10.1016/j.surfcoat.2019.125044.
- [2] G. Tan, J.-H. Lee, Y.-H. Lan, M.-K. Wei, L.-H. Peng, I.-C. Cheng, S.-T. Wu, Broadband antireflection film with moth-eye-like structure for flexible display applications, Optica 4 (2017) 678, https://doi.org/10.1364/optica.4.000678.
- [3] S. Almenabawy, Y. Zhang, A. Flood, R. Prinja, N.P. Kherani, Nanometer-mesa inverted-pyramid photonic crystals for thin silicon solar cells, ACS Appl. Energy Mater. 5 (2022) 13808–13816, https://doi.org/10.1021/acsaem.2c02437.
- [4] D. Przybylski, S. Patela, Modelling of a two-dimensional photonic crystal as an antireflection coating for optoelectronic applications, Opto-Electron. Rev. 27 (2019) 79–89, https://doi.org/10.1016/j.opelre.2019.02.004.
- [5] A. Sharma, T.D. Das, Electronic band structure and optical properties of GaAsSb/GaAs for optoelectronic device applications: a 14 band k.p study, Opt. Mater. (amst) 112 (2021), https://doi.org/10.1016/j.optmat.2020.110734.
- [6] T. Lin, J.n. Xie, S.h. Ning, Q.m. Li, B. Li, Study on the p-type ohmic contact in GaAs-based laser diode, Mater. Sci. Semicond. Process 124 (2021), https://doi.org/10.1016/j.mssp.2020.105622.
- [7] S. Sederberg, F. Kong, F. Hufnagel, C. Zhang, E. Karimi, P.B. Corkum, Vectorized optoelectronic control and metrology in a semiconductor, Nat. Photonics 14 (2020) 680–685, https://doi.org/10.1038/s41566-020-0690-1.
- [8] T. Zaengle, U.J. Gibson, T.W. Hawkins, C. McMillen, B. Ghimire, A.M. Rao, J. Ballato, A novel route to fibers with incongruent and volatile crystalline semiconductor cores: GaAs, ACS Photonics 9 (2022) 1058–1064, https://doi.org/ 10.1021/acsphotonics.2c00008.
- [9] D. Parajuli, G.S. Gaudel, D. Kc, K.B. Khattri, W.Y. Rho, Simulation study of TiO2 single layer anti-reflection coating for GaAs solar cell, AIP Adv. 13 (2023), https://doi.org/10.1063/5.0153197.
- [10] T.C. Lin, Y.T. Chen, Y.F. Yin, Z.X. You, H.Y. Kao, C.Y. Huang, Y.H. Lin, C.T. Tsai, G. R. Lin, J.J. Huang, Large-signal modulation performance of light-emitting diodes with photonic crystals for visible light communication, IEEE Trans. Electron Devices 65 (2018) 4375–4380, https://doi.org/10.1109/TED.2018.2864346.
- [11] G. Oh, Y. Kim, S.J. Lee, E.K. Kim, Broadband antireflective coatings for high efficiency InGaP/GaAs/InGaAsP/InGaAs multi-junction solar cells, Sol. Energy Mater. Sol. Cells 207 (2020), https://doi.org/10.1016/j.solmat.2019.110359.

- [12] W. Zhang, K. Hu, J. Tu, A. Aierken, D. Xu, G. Song, X. Sun, L. Li, K. Chen, D. Zhang, Y. Zhuang, P. Xu, H. Wu, Broadband graded refractive index TiO2/Al2O3/MgF2 multilayer antireflection coating for high efficiency multi-junction solar cell, Sol. Energy 217 (2021) 271–279, https://doi.org/10.1016/j.solener.2021.01.012.
- [13] G.J. Hou, I. García, I. Rey-Stolle, High-low refractive index stacks for broadband antireflection coatings for multijunction solar cells, Sol. Energy 217 (2021) 29–39, https://doi.org/10.1016/j.solener.2021.01.060.
- [14] M.A. Zahid, M.Q. Khokhar, Z. Cui, H. Park, J. Yi, Improved optical and electrical properties for heterojunction solar cell using Al2O3/ITO double-layer antireflective coating, Results Phys. 28 (2021), https://doi.org/10.1016/j. rinp.2021.104640.
- [15] T. Sertel, Y. Ozen, V. Baran, S. Ozcelik, Effect of single-layer Ta2O5 and double-layer SiO2/Ta2O5 anti-reflective coatings on GaInP/GaAs/Ge triple-junction solar cell performance, J. Alloy. Compd. 806 (2019) 439–450, https://doi.org/10.1016/j.iallcom.2019.07.257.
- [16] S. Ji, K. Song, T.B. Nguyen, N. Kim, H. Lim, Optimal moth eye nanostructure array on transparent glass towards broadband antireflection, ACS Appl. Mater. Interfaces 5 (2013) 10731–10737, https://doi.org/10.1021/am402881x.
- [17] F. Galeotti, F. Trespidi, G. Timò, M. Pasini, Broadband and crack-free antireflection coatings by self-assembled moth eye patterns, ACS Appl. Mater. Interfaces 6 (2014) 5827–5834, https://doi.org/10.1021/am500687f.
- [18] Hung, Yung-Jr, San-Liang Lee, and Larry A. Coldren, Deep and tapered silicon photonic crystals for achieving anti-reflection and enhanced absorption, Opt. Express 18.7 (2010), 6841-6852. doi.org/10.1364/OE.18.006841.
- [19] H.K. Raut, V.A. Ganesh, A.S. Nair, S. Ramakrishna, Anti-reflective coatings: a critical, in-depth review, Energ. Environ. Sci. 4 (2011) 3779–3804, https://doi. org/10.1039/c1ee01297e
- [20] M.A. Zahid, M.Q. Khokhar, S. Park, S.Q. Hussain, Y. Kim, J. Yi, Influence of Al2O3/ IZO double-layer antireflective coating on the front side of rear emitter silicon heterojunction solar cell, Vacuum 200 (2022), https://doi.org/10.1016/j. vacuum 2022 110967
- [21] M.A. Zahid, M.Q. Khokhar, Y. Kim, J. Yi, Utilization of CaF2/TTO double-layer antireflective coating for increasing the efficiency in rear emitter SHJ solar cells, Cryst. Res. Technol. 57 (2022), https://doi.org/10.1002/crat.202100233.
- [22] Y.S. Lee, L.Y. Chuang, C.J. Tang, Z.Z. Yan, B.S. Le, C.C. Jaing, Investigation into the characteristics of double-layer transparent conductive oxide ITO/TNO antireflection coating for silicon solar cells, Crystals (Basel) 13 (2023), https://doi.org/ 10.3390/cryst13010080.
- [23] N. Sahouane, A. Zerga, Optimization of antireflection multilayer for industrial crystalline silicon solar cells, Energy Procedia (2014) 118–125, https://doi.org/ 10.1016/j.egypro.2013.12.017.
- [24] A.H. Chiou, C.W. Chang, C.J. Ting, Spectrally selective antireflection of nanoimprint lithography-formed 3D spherical structures on film coated with a silver layer, Sci. Rep. 12 (2022), https://doi.org/10.1038/s41598-022-23348-w.
- [25] L. Dong, Z. Zhang, R. Ding, L. Wang, M. Liu, Z. Weng, Z. Wang, D. Li, Controllable superhydrophobic surfaces with tunable adhesion fabricated by laser interference lithography, Surf. Coat. Technol. 372 (2019) 434–441, https://doi.org/10.1016/j. surfacet 2019 05 039
- [26] L. Dong, Z. Zhang, L. Wang, Z. Weng, M. Ouyang, Y. Fu, J. Wang, D. Li, Z. Wang, Fabrication of hierarchical moth-eye structures with durable superhydrophobic property for ultra-broadband visual and mid-infrared applications, Appl. Opt. 58 (2019) 6706, https://doi.org/10.1364/ao.58.006706.
- [27] T. Sridarshini, S. Indira Gandhi, Photonic band structure of 2D photonic crystals A comparative study, Laser Phys. 30 (2020), https://doi.org/10.1088/1555-6611/ phg705
- [28] K. Wang, X. Dong, Y. Bu, X. Wang, Design of photonic crystals for light-emitting diodes, J. Am. Ceram. Soc. (2023), https://doi.org/10.1111/jace.19388.
- [29] L. Suslik, D. Pudis, M. Goraus, R. Nolte, J. Kovac, J. Durisova, P. Gaso, P. Hronec, P. Schaaf, Photonic crystal and photonic quasicrystal patterned in PDMS surfaces

- and their effect on LED radiation properties, Appl. Surf. Sci. 395 (2017) 220–225, https://doi.org/10.1016/j.apsusc.2016.07.051.
- [30] M.A. Husanu, C.P. Ganea, I. Anghel, C. Florica, O. Rasoga, D.G. Popescu, Surface topography to reflectivity mapping in two-dimensional photonic crystals designed in germanium, Appl. Surf. Sci. 355 (2015) 1186–1191, https://doi.org/10.1016/j. apsusc.2015.07.218.
- [31] H. Kaviani, J. Barvestani, Photonic crystal based biosensor with the irregular defect for detection of blood plasma, Appl. Surf. Sci. 599 (2022), https://doi.org/ 10.1016/j.apsusc.2022.153743.
- [32] S.Y. Kanamori, M. Sasaki, K. Hane, Broadband antireflection gratings fabricated upon silicon substrates, Opt. Lett. 24 (20) (1999) 1422–1424, https://doi.org/ 10.1364/OL.24.001422.
- [33] J. Li, J. Yan, L. Jiang, J. Yu, H. Guo, L. Qu, Nanoscale multi-beam lithography of photonic crystals with ultrafast laser, Light Sci. Appl. 12 (2023), https://doi.org/ 10.1038/s41377-023-01178-3.
- [34] K.J. Byeon, S.Y. Hwang, H. Lee, Fabrication of two-dimensional photonic crystal patterns on GaN-based light-emitting diodes using thermally curable monomerbased nanoimprint lithography, Appl. Phys. Lett. 91 (2007), https://doi.org/ 10.1063/1.2776980
- [35] M. Torras, P. Molet, L. Soler, J. Llorca, A. Roig, A. Mihi, Au/TiO2 2D-photonic crystals as UV-visible photocatalysts for H2 production, Adv. Energy Mater. 12 (2022), https://doi.org/10.1002/aenm.202103733.
- [36] H. Zhao, X. Cao, Q. Dong, C. Song, L. Wang, L. Gao, Large-area silicon photonic crystal supporting bound states in the continuum and optical sensing formed by nanoimprint lithography, Nanoscale Adv. 5 (2023) 1291–1298, https://doi.org/ 10.1039/d3na00001i.
- [37] N. Pérez, T. Tavera, A. Rodríguez, M. Ellman, I. Ayerdi, S.M. Olaizola, Fabrication of sub-micrometric metallic hollow-core structures by laser interference lithography, Appl. Surf. Sci., Elsevier B.V., 2012, pp. 9370–9373, doi: 10.1016/j. apsusc.2012.03.185.
- [38] M. Ellman, A. Rodríguez, N. Pérez, M. Echeverria, Y.K. Verevkin, C.S. Peng, T. Berthou, Z. Wang, S.M. Olaizola, I. Ayerdi, High-power laser interference lithography process on photoresist: effect of laser fluence and polarisation, Appl. Surf. Sci. 255 (2009) 5537–5541, https://doi.org/10.1016/j.apsusc.2008.07.201.
- [39] Y.R. Wang, I.S. Han, C.Y. Jin, M. Hopkinson, Precise arrays of epitaxial quantum dots nucleated by in situ laser interference for quantum information technology applications, ACS Appl. Nano Mater. 3 (2020) 4739–4746, https://doi.org/ 10.1021/acsamm.0c00738.
- [40] L. Dong, Z. Zhang, Z. Wang, D. Li, M. Liu, Design an asymmetrical three-beam laser interference lithography for fabricating micro- and nano-structures, J. Laser Micro Nanoeng, 15 (2020) 85–91, https://doi.org/10.2961/jlmn.2020.02.2002.
- [41] I. Martín-Fabiani, S. Riedel, D.R. Rueda, J. Siegel, J. Boneberg, T.A. Ezquerra, A. Nogales, Micro- and submicrostructuring thin polymer films with two and threebeam single pulse laser interference lithography, Langmuir 30 (2014) 8973–8979, https://doi.org/10.1021/la5021059.
- [42] I. Castro-Hurtado, T. Tavera, P. Yurrita, N. Pérez, A. Rodriguez, G.G. Mandayo, E. Castaño, Structural and optical properties of WO 3 sputtered thin films nanostructured by laser interference lithography, Appl. Surf. Sci. 276 (2013) 229–235, https://doi.org/10.1016/j.apsusc.2013.03.072.
- [43] Y.-R. Wang, S.M. Olaizola, I.S. Han, C.-Y. Jin, M. Hopkinson, Direct patterning of periodic semiconductor nanostructures using single-pulse nanosecond laser interference, Opt. Express 28 (2020) 32529, https://doi.org/10.1364/oe.397709.
- [44] M. Qiu, S. He, Large complete band gap in two-dimensional photonic crystals with elliptic air holes, Phys. Rev. B: Condens. Matter Mater. Phys. 60 (1999) 10610–10612, https://doi.org/10.1103/PhysRevB.60.10610.
- [45] S. Behera, P.W. Fry, H. Francis, C.Y. Jin, M. Hopkinson, Broadband, wide-angle antireflection in GaAs through surface nano-structuring for solar cell applications, Sci. Rep. 10 (2020), https://doi.org/10.1038/s41598-020-63327-7.